Supporting Information
Proton transverse relaxation as a sensitive probe for structure determination in solid proteins

Petra Rovó, Kristof Grohe, Karin Giller, Stefan Becker, Rasmus Linser*

Max Planck Institute for Biophysical Chemistry, Göttingen

Supplementary Discussion

Calibration of PRE restraints

Similar to NOE data, under non-ideal conditions (background effects, ^{1}H spin diffusion, mobility of spin label etc.) the PRE data need to be calibrated based on known distances to facilitate the convergence of a structure calculation process. In contrast to NOE data, however, no long distances of known values are usually present. Calibration of the initial uncalibrated PRE data can be pursued also in an iterative way using a set of distances that are only approximately known (see Figure S7). In our case, a low-resolution structure based on a sparse set of RFDR data, or even only the secondary structure element to which the spin label is attached, is sufficient to obtain initial calibration values. Using the average structure of this structural bundle, we can determine expected distances between the spin label and single amide groups. In particular, the β-strands preceding and following the spin label expectedly present a series of amino acids with almost linearly increasing distances from the spin label (red diamonds in Figure S7). We can derive a tentative linear fit of the correlation between uncorrected PRE-derived distances and the distances expected on the basis of the initial low-resolution structure to derive an approximate correction. This correction is applied going from a) to b) in Figure S7. Using the corrected PRE distances in addition to the RFDR restraints, we obtain an improved structural ensemble. Iteratively the correction could be repeated to yield more accurate PRE-derived distance restraints for a final structural ensemble. Under the conditions chosen here (using a starting structure based of 23 short distance RFDR restraints and 69 dihedral angle restraints), the initial (tentative) correction values (slope of 0.13 ± 0.03 and intercept of 12.1 ± 0.7 Å) already very similar to the „true" correction values (slope of 0.16 ± 0.02 and intercept of 11.5 ± 0.4 Å). The true correction values—as described in the main text—were derived from a more accurate starting structure based on all RFDR restraints available.

Paramagnetic Relaxation Enhancement (PRE)

The stochastical modulation of the dipole-dipole (DD) coupling between an unpaired electron and a nuclear magnetic moment induces nuclear relaxation in a distance-dependent manner as described by the Solomon equations:

$$\Gamma_1^{\mathrm{DD}} = \frac{2}{15}\left(\frac{\mu_0}{4\pi}\right)^2 \frac{\gamma_I^2 g_e^2 \mu_{\mathrm{B}}^2 S(S+1)}{r^6} \times \left[\frac{\tau_c}{1+(\omega_I-\omega_e)^2\tau_c^2} + \frac{3\tau_c}{1+\omega_I^2\tau_c^2} + \frac{6\tau_c}{1+(\omega_I+\omega_e)^2\tau_c^2}\right], \tag{1}$$

$$\Gamma_2^{\mathrm{DD}} = \frac{1}{15}\left(\frac{\mu_0}{4\pi}\right)^2 \frac{\gamma_I^2 g_e^2 \mu_{\mathrm{B}}^2 S(S+1)}{r^6} \times \left[4\tau_c + \frac{\tau_c}{1+(\omega_I-\omega_e)^2\tau_c^2} + \frac{3\tau_c}{1+\omega_I^2\tau_c^2} + \frac{6\tau_c}{1+(\omega_I+\omega_e)^2\tau_c^2} + \frac{6\tau_c}{1+\omega_e^2\tau_c^2}\right], \tag{2}$$

where μ_0 is the vacuum permeability, γ_I is the gyromagnetic ratio of a nucleus, g_e is the free electron g factor, μ_{B} is the Bohr magneton, S is the electron spin angular momentum, r is the electron-nucleus distance, ω_I is the nuclear Larmor frequency, ω_e is the electron Larmor frequency, and τ_c is the correlation time of the relaxation mechanism. This correlation time is determined by the fastest process among electron relaxation, chemical exchange or molecular tumbling:

$$\tau_c = (\tau_e^{-1} + \tau_m^{-1} + \tau_r^{-1})^{-1}, \tag{3}$$

where τ_e is the electron relaxation time, τ_m is the time constant for chemical exchange and τ_r is the molecular reorientational correlation time. In the solid state the electron-nucleus DD relaxation depends primarily on the electron spin relaxation time, while chemical exchange and overall tumbling have negligible contribution to the relaxation rates, thus the correlation time in equation 1 and 2 can be replaced by τ_e.

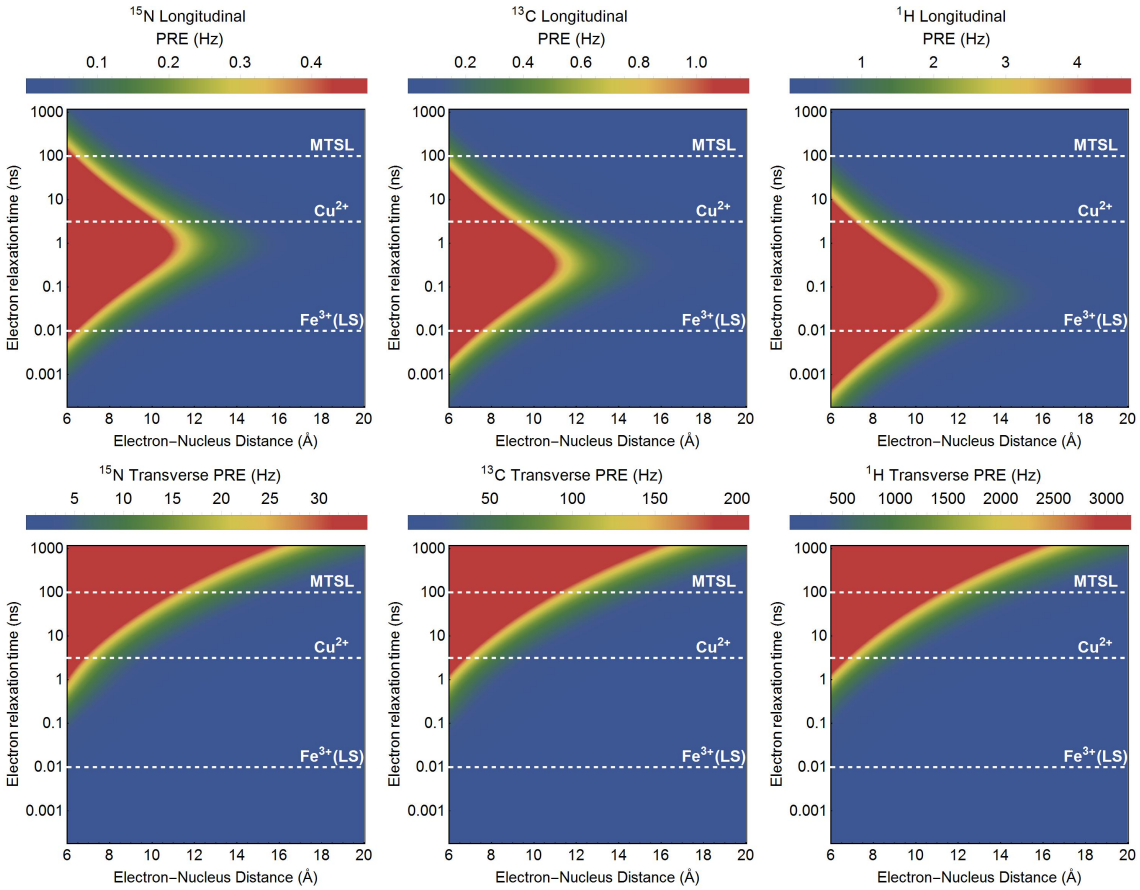

Figure S1: Longitudinal (top) and transverse (bottom) relaxation rate enhancements as a function of electron relaxation time (τ_e) and electron-nucleus distance (r) for ^{15}N, ^{13}C and ^{1}H nuclei at 18.79 T magnetic field strength (800 MHz ^{1}H frequency), for $S = 1/2$ spins calculated with equation 1 and 2. Dashed lines indicate the electron relaxation times of MTSL nitroxide spinlabel (100 ns), Cu^{2+} ion (3 ns) and low-spin Fe^{2+} ion (10 ps).

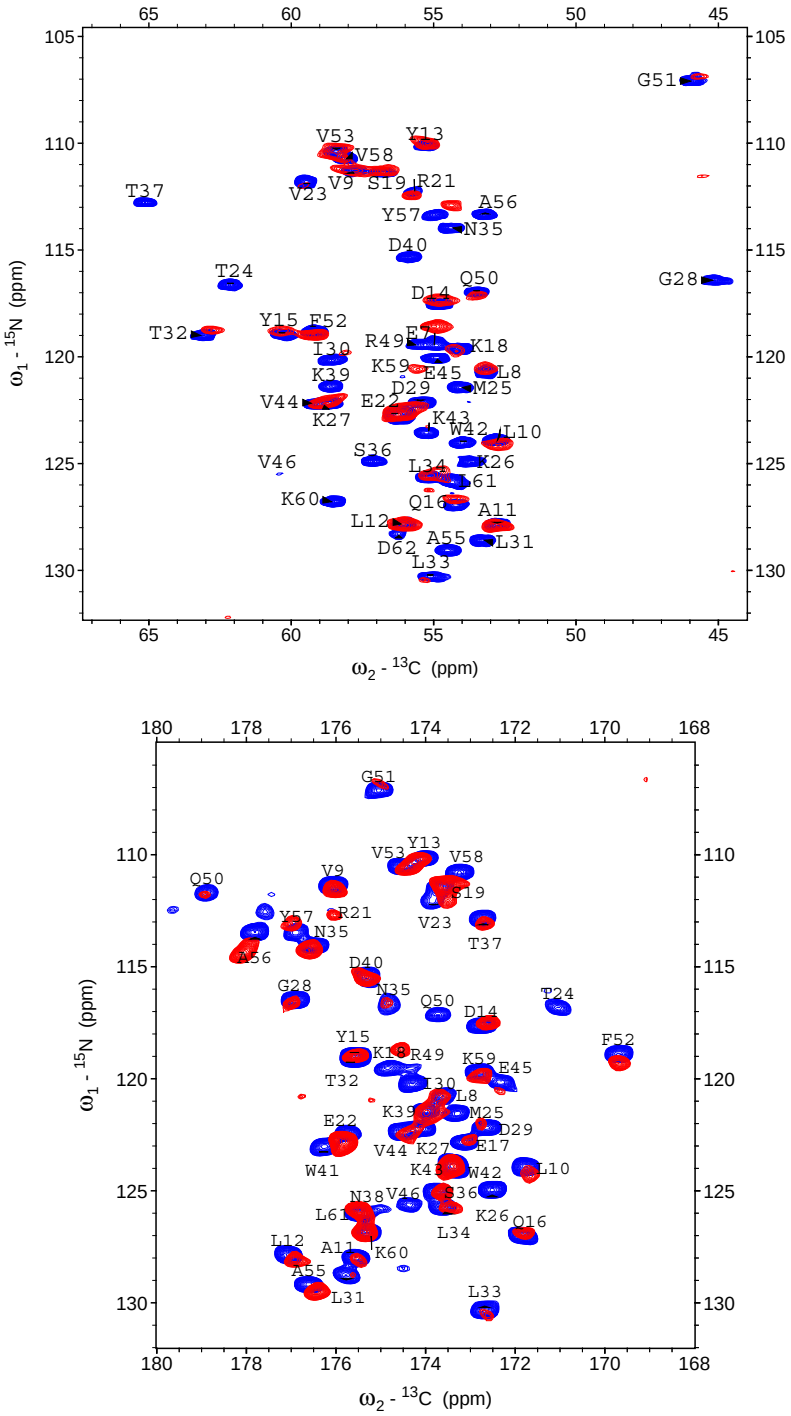

Figure S2: Upper panel: Solid-state $^{13}C\alpha$-^{15}N correlation spectra of protonated, ^{13}C, ^{15}N labeled diamagnetic SH3 (blue) and protonated, ^{13}C, ^{15}N, non-diluted, MTSL-labeled, paramagnetic SH3 (red), recorded at 800 MHz ^{1}H Larmor frequency at 55.55 kHz MAS. Lower panel: Solid-state ^{15}N-^{13}CO correlation spectra of perdeuterated, 100% amide proton back-exchanged diamagnetic (blue) and paramagnetic, MTSL-labeled (red) SH3, recorded at 800 MHz ^{1}H Larmor frequency at 55.55 kHz MAS.

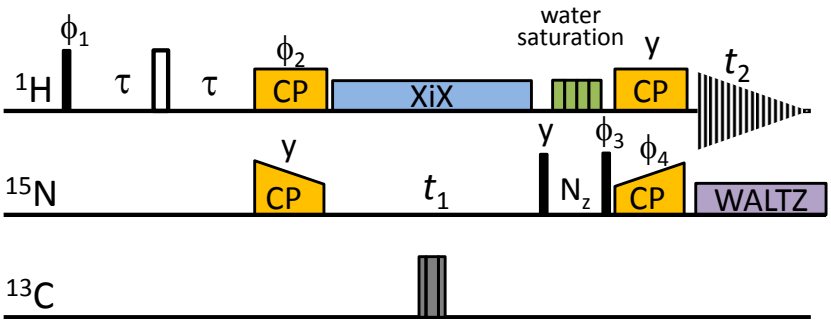

Figure S3: Pulse scheme for ^{1}H transverse relaxation rate measurements. Filled (open) symbols denote 90° (180°) pulses and were applied at 55, 35 and 55 kHz field strength for ^{1}H, ^{15}N and ^{13}C channels, respectively, with phase x unless otherwise stated. Cross-polarization (CP) between ^{1}H and ^{15}N was accomplished using a rectangular 20 kHz pulse on ^{1}H and tangential 36 kHz pulse on ^{15}N with a duration of 900 μs. High-power ^{1}H, ^{13}C and ^{15}N 90° pulse lengths were 4.5 μs, 4.5 μs and 7.0 μs, respectively. τ denotes the relaxation delay for relaxation rate measurements. During ^{15}N evolution, 14 kHz low-power XiX was applied [1]. Suppression of the water signal was achieved using the MISSISSIPPI scheme [2]. During acquisition ^{15}N WALTZ decoupling was applied at 2.5 kHz. Quadratura detection in t_1 was achieved by alternating the pulse phase following the t_1 evolution according to the TPPI scheme. The phase cycle was ϕ_1: x,-x; ϕ_2: $8 \cdot$x,$8 \cdot$-x; ϕ_3: $2 \cdot$x,$2 \cdot$-x; ϕ_4: $4 \cdot$x,$4 \cdot$-x and the receiver phase cycle was x,-x,-x,x, -x,x,x,-x, -x,x,x,-x, x,-x,-x,x.

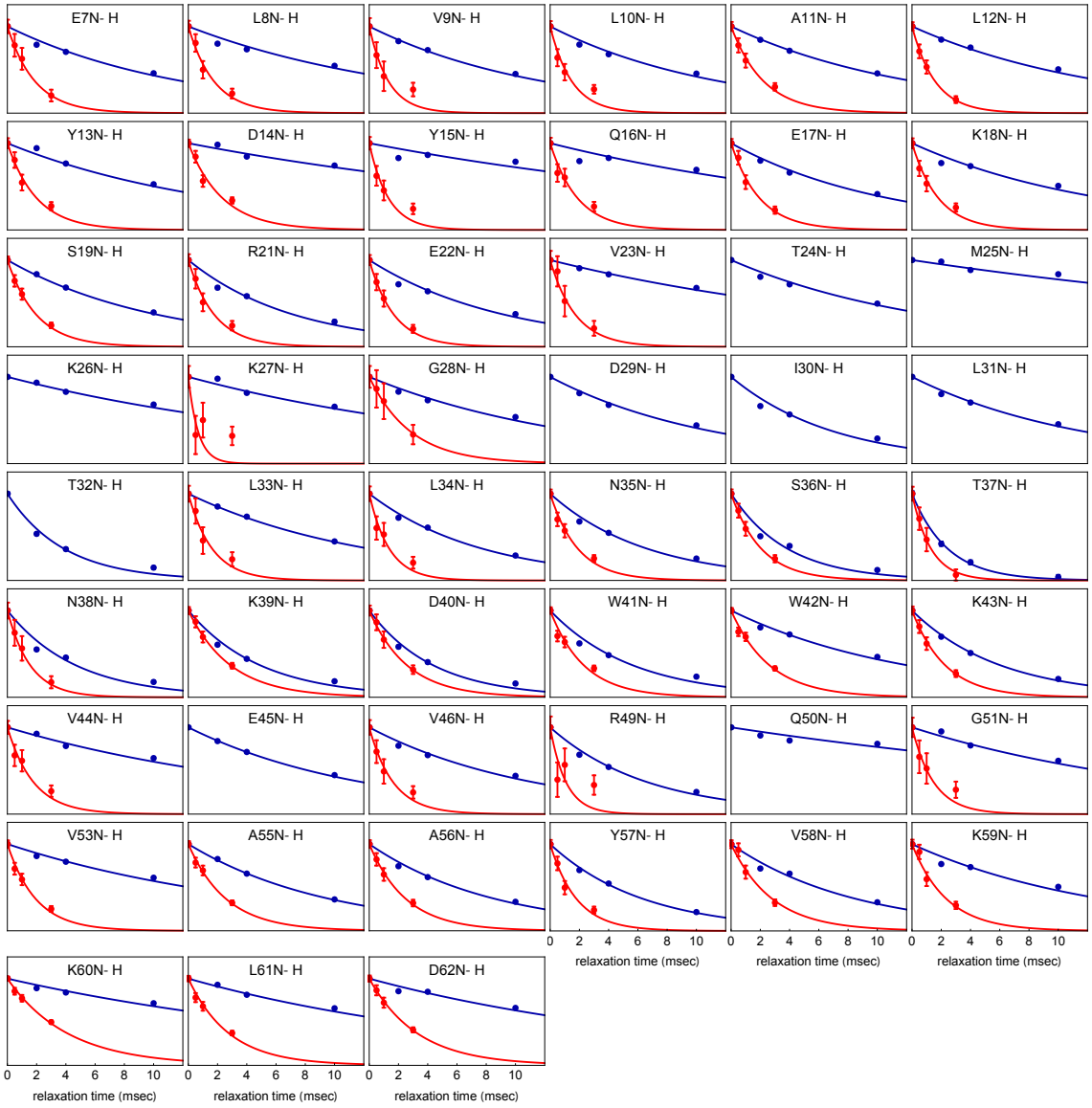

Figure S4: Measured ^{1}H transverse relaxation decay curves of perdeuterated, 100% amide proton back-exchanged diamagnetic (blue) and MTSL-labeled paramagnetic (red) SH3. Experimental data were fitted with a single exponential and these are shown as solid lines with the corresponding color. Error bars indicate experimental uncertainties based on the noise level of the spectra.

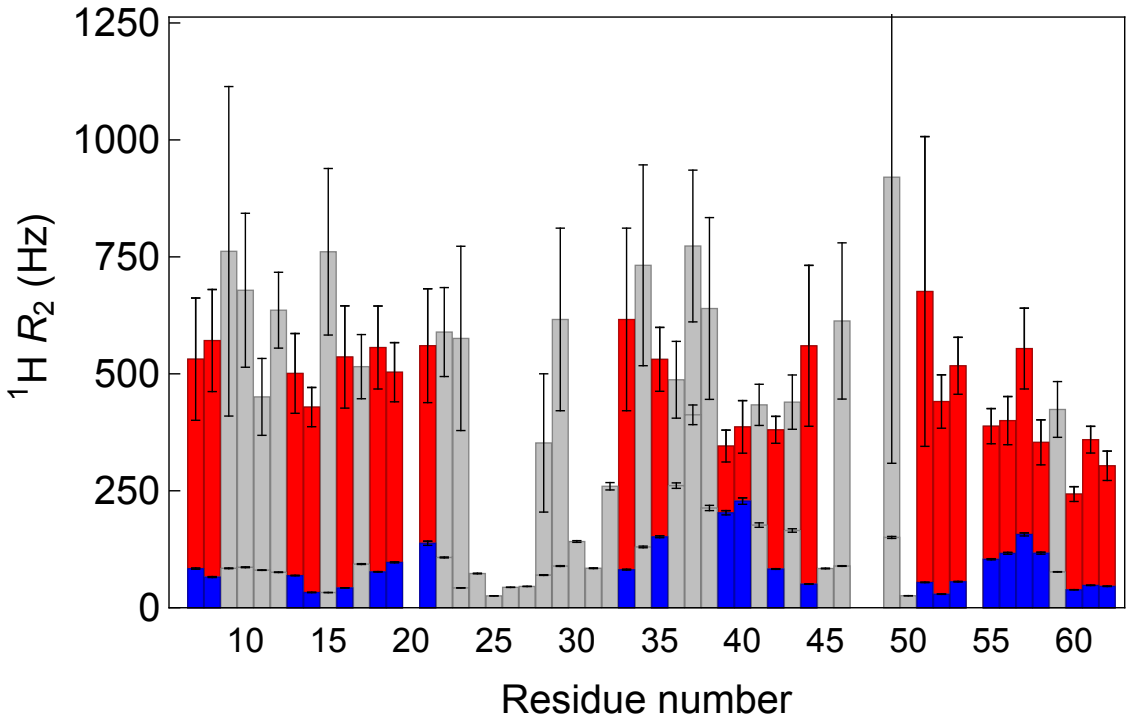

Figure S5: Observed ^{1}H R_2 rates of the diamagnetic (blue) and MTSL-labeled paramagnetic (red) SH3. Error bars represent propageted errors from the noise level of the spectra and from the exponential fit.

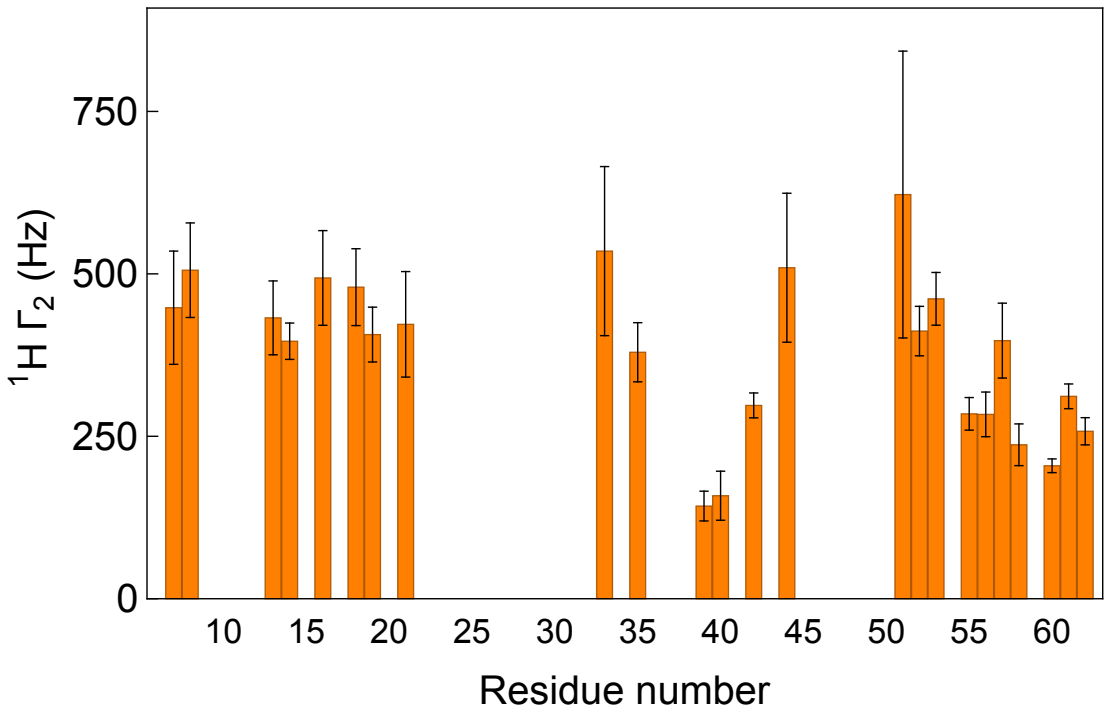

Figure S6: Backbone amide proton transverse paramagnetic relaxation enhancements, Γ_2 as a function of residue number. Γ_2 values were set to zero for those residues where no quantitative measurement could be performed due to peak overlaps or reduced peak intensities.

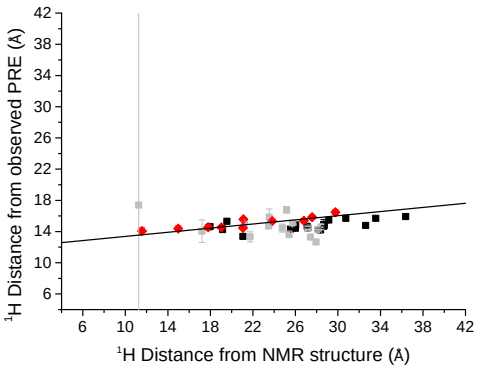

(a) Distance from initial average NMR structure based on short-distance RFDR restraints only vs. distance from uncalibrated PRE.
Slope 0.13 ± 0.03, Interc. 12.1 ± 0.7 Å, $R^2 = 0.64$

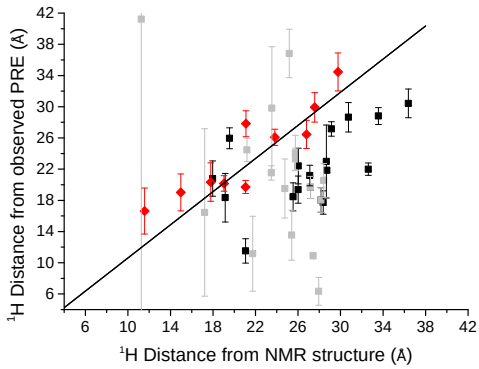

(b) Distance from initial average NMR structure based on short-distance RFDR restraints only vs. distance from calibrated PRE.

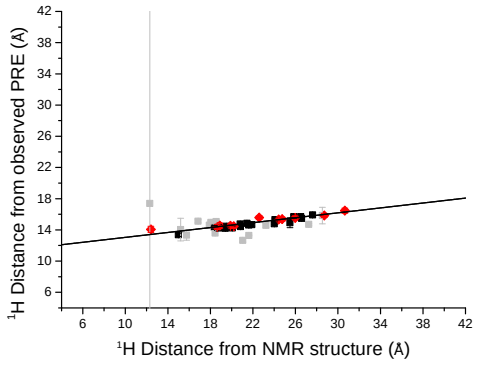

(c) Distance from final average NMR structure based on short- and long-distance RFDR restraints vs. distance from uncalibrated PRE.
Slope 0.16 ± 0.02, Interc. 11.5 ± 0.4 Å, $R^2 = 0.82$

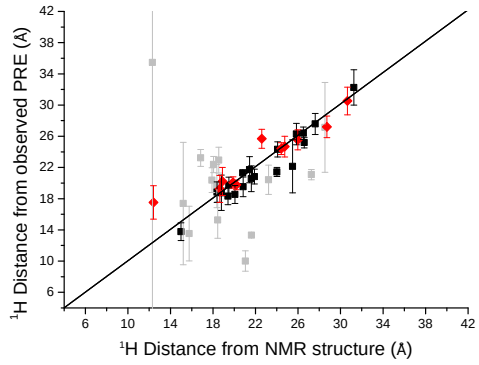

(d) Distance from final average NMR structure based on short- and long-distance RFDR restraints vs. distance from calibrated PRE.

Figure S7: Agreement between experimentally obtained, PRE derived distances and distances from calculated NMR structures. In (a) and (b) the NMR structures were calculated by using 23 short-distance ^{1}H-^{1}H RFDR restraints ($d_{\mathrm{H}_i\mathrm{H}_j} \leq 4$ Å) and 69 dihedral angle restraints. In (c) and (d) the NMR structures were calculated by using 29 long-distance ^{1}H PRE, 294 ^{1}H-^{1}H RFDR distance restraints and 69 dihedral angle restraints. Red diamonds represent the residues of the β-strands preceding and following the MTSL tag, which were used to calibrate the system. Gray points represent the ambiguous, overlapping peaks which were left out from the later structure calculation. After calibration the slope and intercept are 1 and 0, respectively, with an unchanged R^2 value.

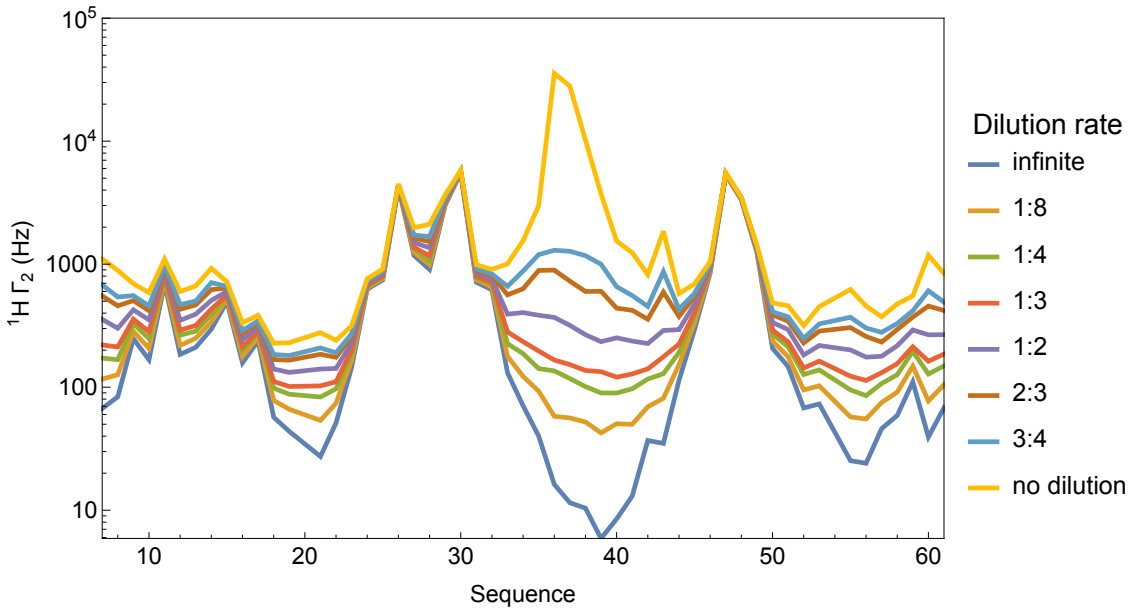

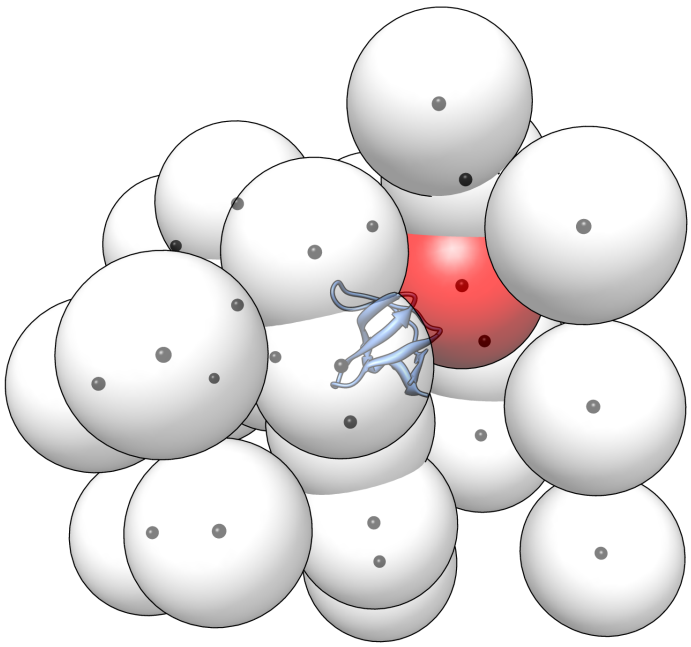

Figure S8: Simulated ^{1}H transverse PRE of SH3 amide protons at different dilution rates (upper panel). For the simulations the crystal lattice was modeled using 25 structures (lower panel), and the amide proton relaxation of the central molecule (displayed with ribbon) was assumed to be affected only by its own paramagnetic tag (red sphere) and by the unpaired electrons of the 24 surrounding molecules (white spheres) and no other effects were considered. Infinite dilution reflects the solution state PRE, and no dilution represents the solid state PRE where all proteins in the crystal lattice are paramagnetically tagged. In all intermediate cases the paramagnetic protein senses a stochastic distribution of paramagnetic effects coming from the paramagnetic and diamagnetic neighbors.

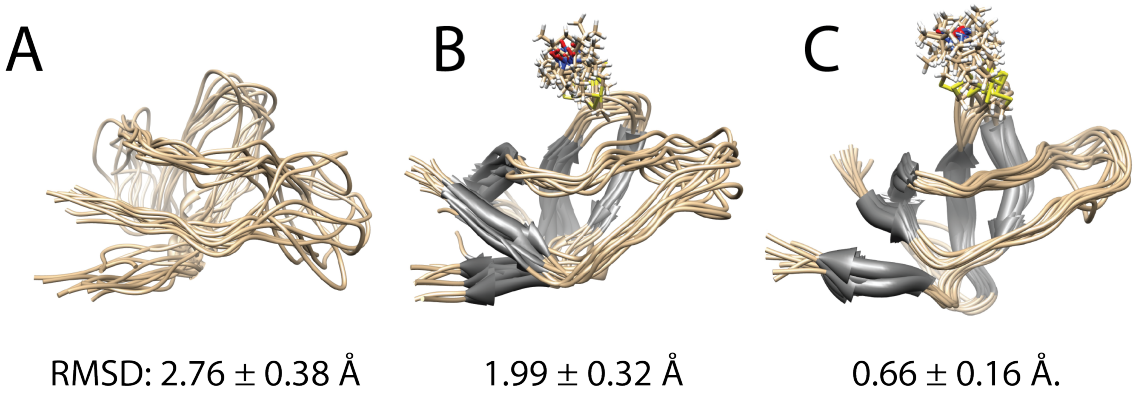

Figure S9: Structure ensemble of SH3 obtained using (*A*) 69 dihedral angles and 23 short-distance RFDR restraints; (*B*) same restraints used as in *A* but including 29 PRE restraints; (*C*) same restraints used as in *B* but including all 294 RFDR restraints. Mean backbone RMSD of the structured region (residues 8-16, 24-34, 42-46, 49-57) are given below the structure bundles. The backbone RMSDs with respect to the X-ray structure are (*A*) 4.78 ± 0.33 Å (*B*) 4.53 ± 0.30 Å and (*C*) 1.90 ± 0.10 Å.

Table S1: ^{1}H PRE restraints as defined between the MTSL nitroxide oxygen and the amide proton of the listed residues.

Residue	Lower dist Å	Upper dist Å
	Type 1 restraints	
7	18.72	20.72
8	17.45	19.65
13	19.83	21.83
14	21.02	24.42
16	18.22	20.82
18	16.62	20.02
19	20.32	22.32
21	17.44	20.24
33	16.46	21.06
35	23.32	25.32
39	29.95	34.55
40	28.72	32.32
42	23.61	25.21
44	18.42	22.02
51	17.05	21.45
52	18.89	21.29
53	18.78	20.78
55	23.37	25.97
56	24.49	25.89
57	21.64	29.64
58	24.88	27.68
60	25.60	27.20
61	21.34	25.34
62	26.23	28.93
	Type 2 restraints	
24	1.80	15.00
29	1.80	15.00
30	1.80	15.00
45	1.80	15.00
50	1.80	15.00

Table S2: NMR and refinement statistics for SH3 structure.

NMR distance and dihedral constraints	
Distance restraints	
Total RFDR	294
Intra-residue:	28
Inter-residue	262
Sequential (|i - j| = 1)	58
Medium-range (|i - j| < 4)	47
Long-range (|i - j| > 5)	147
Intermolecular	0
Hydrogen bonds	0
Total PRE restraints	29
Total dihedral angle restraints	69
ϕ	34
ψ	35
Structure statistics	
Violations (mean and s.d.)	
Distance restraints (Å)	0.15 ± 0.02
Dihedral angle restraints (°)	16.4 ± 0.02
Ramachandran Statistics (%)	
most favored regions	72.2
allowed regions	23.5
generously allowed regions	3.9
disallowed regions	0
Deviations from idealized geometry	
Bond lengths (Å)	$(7 \pm 0.3)10^{-4}$
Bond angles (°)	0.3 ± 0.003
Impropers (°)	0.16 ± 0.006
Average pairwise r.m.s. deviation* (Å)	
Heavy atoms (8-17, 23-58)	1.92 ± 0.37
Backbone atoms (8-17, 23-58)	0.84 ± 0.20

* Pairwise r.m.s. deviation was calculated among 10 refined structures.

References

[1] M. Ernst, A. Samoson, B. H. Meier, *J Magn Reson* **2003**, *163*, 332–339.

[2] D. H. Zhou, C. M. Rienstra, *J Magn Reson* **2008**, *192*, 167–172.